Inorganic Chemistry

Article

pubs.acs.org/IC

Slow Spin Dynamics between Ferromagnetic Chains in a Pure-Inorganic Framework

Rénald David,[†] Houria Kabbour,[†] Silviu Colis,[‡] and Olivier Mentré[†,*]

[†]UMR 8181 CNRS, Unité de Catalyse et de Chimie du Solide (UCCS USTL), Université Lille Nord de France, F-59655 Villeneuve d'Ascq, France

[‡]Institut de Physique et Chimie des Matériaux de Strasbourg (IPCMS), UMR 7504 CNRS and Université de Strasbourg (UDS-ECPM), F-67034 Strasbourg Cedex 2, France

Supporting Information

ABSTRACT: The crystal structure of the new phase $BaCo^{II}_2(As^{III}_3O_6)_2{\cdot}2(H_2O)$ is built from the stacking of infinite $[BaCo_2(As_3O_6)_2{\cdot}H_2O]$ sheets containing $_\infty[Co^{II}O_4]^{6-}$ chains interconnected by perpendicular $_\infty[As^{III}O_2]^-$ chains. It shows a metamagnetic transition below ~9 K at a critical field of ~0.11 T, leading to a moment value of 70% of the expected saturation, related to the spin flip between individual robust canted ferromagnetic chains. We propose a field-dependent scenario with magnetic moments lying in the $Co^{II}O_6$ octahedral basal planes, fully compatible with our experimental results. Magnetic measurements under *ac*-field show slow spin dynamics with an intrinsic single-chain magnet (SCM)-like component slightly modified in the field-aligned regime. The characteristic relaxation time and energy barrier are about $\tau_o = 5.1 \times 10^{-10}$ s and $\Delta_\tau = 35.3$ K at $H_{dc} = 0$, respectively, which falls close to values found for other (but organometallic) SCM Co^{II} chains. This magnetic behavior is unique in the field of pure-inorganic compounds.

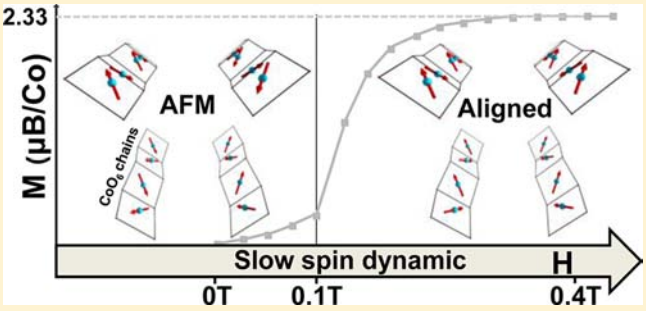

INTRODUCTION

Is it possible to reach the same degree of disconnection between magnetic units of molecular magnets using inorganic spacers? Indeed, low-dimensional magnetic oxides are of increasing interest due to the peculiar properties and the versatile interplay between magnetic clusters and an external magnetic field. Exotic fundamental states and other phenomena such as field-induced transitions or magnetization steps can be expected, especially when strong magnetocrystalline anisotropy is involved.[1−3] The latter raises from strong magnetocrystalline anisotropy favored, for instance, by ions such as Co^{II}, Co^{III}, and Fe^{II} with strong spin−orbit couplings. It follows that, in the case of ideally decoupled ferromagnetic subunits, i.e., using large organic spacers, the expected behaviors cover slow magnetic relaxation and magnetic hysteresis found in single-molecular magnets (SMMs)[4,5] and single-chain magnets (SCMs).[6−8] Rational synthesis strategies have been developed in the past decade[9] to conceive such molecular magnetic compounds for future memory nanodevices or recording media. Concerning pure-inorganic materials, greater thermal stability and easier handling and deposition could be expected, compared to molecular/metal hybrid materials, while the efficient disconnection of magnetic units remains a challenging barrier. In this context, we are greatly interested in novel compounds of the BaO-X_2O_5 (X = P, As)-MO_x (M = Co, Fe) chemical systems due to their capacity to form low-dimensional (1D, 2D) magnetic systems. This choice stems from the large size of Ba^{2+} cations (r = 1.35 Å) and $[X_xO_y]^{n-}$ anions, which are likely to play the role of nonmagnetic spacers. Indeed, both Ba^{II} and XO_4^{3-} spacers are found in the rhombohedral $Ba(M^{II}X^{V}O_4)_2$ (M^{II} = Co, Fe, Ni; X^V = As, P, V) series,[10−14] where honeycomb layers of M^{II} ions are separated by ~8 Å interleaves, leading to a pronounced 2D magnetic behavior. Indeed, $Ba(Co^{II}AsO_4)_2$[12,13] is a good realization of a quasi-2D XY system, while we have recently shown that $Ba(FePO_4)_2$ is the first 2D Ising ferromagnetic oxide.[14] It is noteworthy that, despite the puzzling polymorphism of $Ba(CoPO_4)_2$ with three well-characterized α,β,δ crystal forms,[15] their structural characterization has revealed a full phase diagram dominated by layered structures. In related chemical systems, we note a plethora of other low-D magnetic compounds, such as the realization of 1/3 magnetization steps in CoV_2O_6 due to frustration between 1D-Co^{II} chains[1,2] and in $BaCoX_2O_7$ due to 2D-Co^{II} modulated layers.[16]

In these compounds, X being in its (V) oxidation state, one generally deals with X^VO_4 or $X^V_2O_7$ groups, which interconnect the low-D magnetic units, as in $NH_4CoPO_4{\cdot}H_2O$,[17] $Ba(CoPO_4)_2{\cdot}H_2O$,[18] or $BaFe_2P_2O_7F_2$.[19] In addition, using solvothermal conditions in a reducing medium to ensure stabilization of Fe^{II} or Co^{II} [14] also leads to the co-reduction of As^V into As^{III}, which prefers the $EAsO_3$ coordination (E is the

Received: September 16, 2013
Published: November 18, 2013

   dx.doi.org/10.1021/ic402336n | Inorg. Chem. 2013, 52, 13742−13750

stereoactive As^{III} lone-pair) for X = As compounds. The advantages of these groups in terms of disconnecting spacers is that they can form even more voluminous polyanions, from dimers to tetramers as reviewed in ref 20, due to the additional interaction between E and positive centers. The final disconnection between individual magnetic units could finally be accentuated, as demonstrated in this work. In addition to possible low-D magnetic particularities, the interest of the prospect for new $Ba/Co^{II}/As^{III}$ oxides is reinforced by the single compound $Co^{II}{}_2As^{III}{}_2O_5$ reported so far, to our knowledge.[21] This poor phase diagram most probably arises from the difficulty of combining Co^{II} and As^{III} following common solid-state routes or in standard hydrothermal conditions.

Here we show the preparation of the novel hydrate $BaCo^{II}{}_2(As^{III}{}_3O_6)_2{\cdot}2(H_2O)_2$ formed of infinite chains of edge-sharing Co^{II} octahedra, disconnected by perpendicular $[As^{III}O_2]^-{}_\infty$ chains of corner-sharing AsO_3 triangles. Our magnetic investigation highlights the occurrence of a metamagnetic transition that originates from the spin alignment between robust non-collinear Ising ferromagnetic chains. We show that this compound represents an original metamagnetic system in which strongly disconnected units possess intrinsic slow spin relaxation related to uniaxial anisotropy, which therefore is very similar to what is observed in molecular SCM compounds. This scenario, original in pure-inorganic solid-state chemistry, is based on both experimental results and estimation of coupling exchanges by DFT calculations.

EXPERIMENTAL SECTION

Synthesis. Single crystals of $Co^{II}As^{III}{}_2O_5$, the single (to our knowledge) oxide containing Co^{II} and As^{III}, were obtained as byproduct from the parasitic oxidation of $CoAs_2$ by solid-state route.[21] Indeed, we have already mentioned in ref 14 the possibility to grow $BaFe_2(AsO_4)_2$ and $Fe^{II}As^{III}$ byproducts using a water–hydrazine solution medium. Thus, we performed similar syntheses starting from $BaCO_3$ (0.345 g), $Co^{II}Cl_2$ (0.454 g), and $As^{III}{}_2O_3$ (1.04 g). They were mixed with ∼10 mL of distilled water. Hydrazine (1 mL/85%) was used as reducing agent. The standard redox potentials $E^0{}_{Co(III)/Co(II)}$ = +1.92 V, $E^0{}_{H_3As(V)O_4^{3-}/HAs(III)O_2}$ = +0.58 V, $E^0{}_{N_2/N_2H_5^+}$ = −0.23 V[22] favor the $Co^{III} \rightarrow Co^{II}$ and $As^V \rightarrow As^{III}$ co-reductions. The mixture was poured into a Teflon-lined autoclave, heated to 493 K for 72 h, and then slowly cooled to room temperature during 200 h. Pink transparent needles 1 mm long, corresponding to $BaCo^{II}{}_2(As^{III}{}_3O_6)_2{\cdot}2(H_2O)_2$, were selected from the product, which confirms the efficiency of our redox-active medium using hydrazine in hydrothermal conditions. To obtain single-phase polycrystalline material, we used a microwave-assisted procedure in an adapted Teflon-lined vessel. The amount of starting materials was doubled, and they were mixed in 30 mL of water. The vessel was then heated at 200 °C (power of 300 W) for 30 min and cooled to room temperature in 3 h. The impurities were removed using successive washings with ethanol.

Single-Crystal X-ray Diffraction (XRD). Room-temperature single-crystal XRD was carried out on a DUO-Bruker SMART apex diffractometer using Mo Kα radiation. Intensities were extracted and corrected from the Lorentz-polarization factor through the SAINT program. Multiscan absorption correction was applied using SADABS.[23] The structure was solved using Superflip[24] and refined using Jana2006.[25]

Magnetic Measurements. Data were measured on a MPMS SQUID-VSM (Quantum Design) magnetometer. Prior to any magnetic measurement, powder was magnetically "aligned" in a polymeric gel that freezes the particle orientation below 30 °C. The alignment was performed in a field of 7 T, leading to information along the uniaxial magnetic axis as detailed below. Typical measurements were performed using zero-field-cooling (ZFC) and field-cooling (FC) procedures under 0.02, 0.1, and 0.15 T fields. Magnetization versus field (M/H) variations were measured between 7 and −7 T at different temperatures. Alternating current measurements were carried out between 1.8 and 20 K, at frequencies of 10/33/100/200/330/400/600 Hz without offset field (H_{dc}), and 1/10/33/100/330/997 Hz with H_{dc} = 1 and 1.5 kOe. The driving ac field was 2.5 Oe.

Computational Methods. DFT calculations were performed using the Vienna *ab initio* Simulation Package (VASP).[26] The calculations were carried out within the generalized gradient approximation (GGA+U) for the electron exchange and correlation corrections using the Perdew–Wang[27] functional and the frozen core projected wave vector method.[28] A plane wave energy cutoff of 400 eV, a total energy convergence threshold of 10^{-6} eV, and 50 k-points in the irreducible Brillouin zone were used. The energies of selected ordered spin states can be expressed using the spin Hamiltonian,

$$\hat{H} = -\sum_{i<j} J_{ij}\hat{S}_i{\cdot}\hat{S}_j$$

where J_{ij} corresponds to the exchange parameters between the spin sites i and j, extracted by equating the relative energies of the selected ordered magnetic states to the corresponding energies determined from the GGA+U calculations.

RESULTS AND DISCUSSION

Crystal Structure. The preparation of single crystals of $BaCo^{II}{}_2(As^{III}{}_3O_6)_2{\cdot}2(H_2O)$ is detailed in the Experimental Section. Structure resolution and refinement using single-crystal data led to the following structure parameters: a = 17.978(1) Å, b = 13.939(1) Å, c = 5.9900(4) Å, space group $Pnma$, and reliability factors R = 4.85% and R_w = 6.14% . The structure was solved using the charge-flipping method implemented in Superflip.[24] Oxygen and hydrogen atoms were located on Fourier difference maps and refined without restraints. The crystallographic data and atomic coordinates are summarized in Tables S1 and S2, while selected bond distances are listed in Table 1. $BaCo_2(As_3O_6)_2{\cdot}2(H_2O)_2$ exhibits a 2D

Table 1. Selected Bond Lengths (Å) for $BaCo_2(As_3O_6)_2{\cdot}2(H_2O)_2$

Co1–O1	2.079(9)	Ba1–O1	2 × 2.867(9)
	2.060(9)	–O2	2.926(13)
–O3	2.053(9)	–O5	2 × 2.935(9)
	2.060(9)	–O6	2 × 2.749(9)
–O5	2.375(9)	–O7	2.803 (16)
–O6	2.073(9)	–O8	2.840(16)
		–O9	2.942(15)
As1–O5	1.874(8)		
–O6	1.696 (9)	H1–O9	2 × 0.76(1)
–O7	1.797(7)	H2–O8	2 × 0.86(1)
As2–O1	1.749(9)		
–O2	1.814(7)		
–O4	1.809(9)		
As3–O3	1.739(9)		
–O4	1.786(9)		
–O5	1.850(9)		

structure built from the stacking of infinite $[BaCo_2(As_3O_6)_2{\cdot}H_2O]$ sheets laying in the (b,c) plane, separated by H_2O molecules (Figure 1a). The shortest Co–Co distance across the interleave is 8.93 Å. The sheets are composed of $_\infty[Co^{II}O_4]^{6-}$ chains of edge sharing octahedral (d_{Co-Co} = 3.02 Å) running along the c-direction. The shared edges correspond to the atoms O1 and O3 which belong to the $(O1_2O3_2)$ equatorial plane of each octahedron (Figure 1b). Co atom is shifted out of

dx.doi.org/10.1021/ic402336n | Inorg. Chem. 2013, 52, 13742–13750

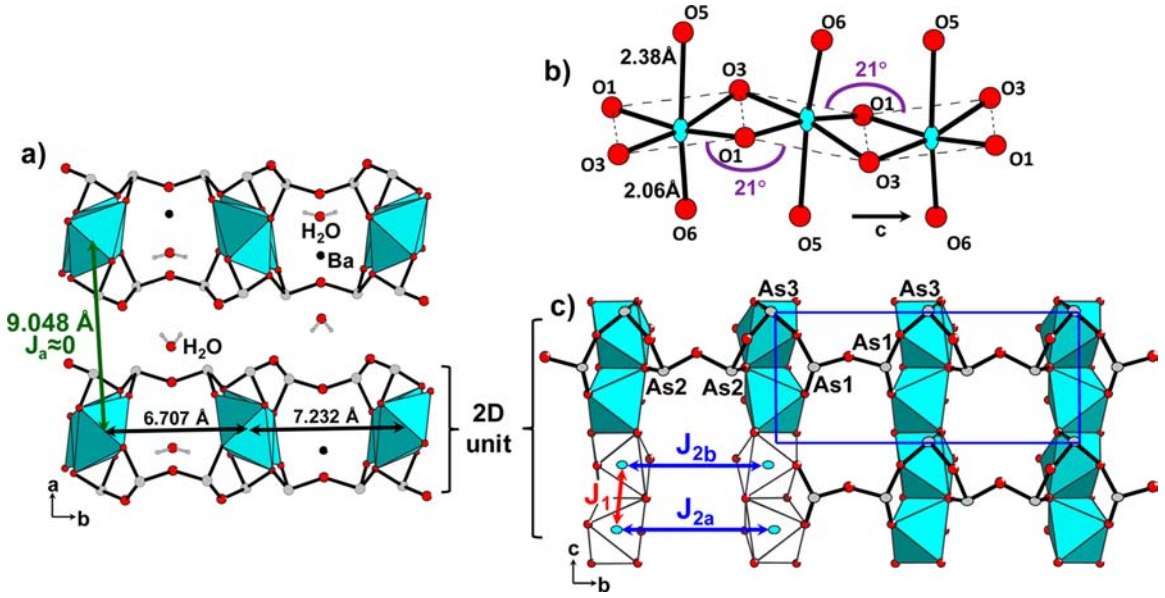

Figure 1. $BaCo_2(As_3O_6)_2 \cdot 2(H_2O)$ structures describing (a) the stacking of $BaCo_2(As_3O_6)_2 \cdot 2(H_2O)$ sheets, (b) the infinite CoO_6 chain, and (c) the 2D sheet in the single-exchange paths.

the equatorial base to form distorted octahedral environment with one long (2.38 Å) Co1−O5 and one short (2.06 Å) Co1−O6 apical bonds. Inside the chains the equatorial planes are tilted by ∼21° from one atom to the next. In the (*b*,*c*) planes two adjacent chains have their "average" equatorial planes tilted by ∼90°, as shown in Figure 1b.

The magnetic chains are interconnected into $(Co_2(As_3O_6)_2)$ sheets (Figure 1c) by $(As^{III}O_2)$ chains of corner-sharing $EAs^{III}O_3$ tetrahedra, where E corresponds to the stereoactive As^{III} lone-pair. These zigzag chains growing along *b* are formed of three independent As atoms arranged into the (O-As1-O-As1-O-As3-O-As2-O-As2-O-As3-) sequence. Dimeric fragments $As1_2O_5$ and $As2_2O_5$ play the roles of spacers between the Co^{II} chains, while As_3O_3 is located at the vertices of the chains, as shown on the Figure 1c. This connection at both sides of the octahedral chains forces a tilt between adjacent chains (∼90°) to bring closer/longer the apical CoO_6 corners when the connection is performed by $As1_2O_5/As2_2O_5$. There is a diversity of topologies that can be created by corner-sharing of AsO_3 subunits, as reviewed in ref 20. For instance, dimeric As_2O_5 units have already been evidenced in $Pb_8OCl_6(As_2O_5)_2$[29] and can also accept the co-presence of other groups such as tetrameric rings in $M_4(As_2O_5)_2(As_4O_8)$ (M = Nd, Sm).[30] However, $_\infty[AsO_2]^-$ chains (*or catena-arsenites*) are rather rare, even if found in very simple oxides such as $NaAsO_2$,[31] the mineral leiteite $ZnAs_2O_4$,[32] the hybrid compounds $(H_3NCH_2CH_2NH_3)_{0.5}[AsO_2]$,[31] or the more complex (As_2O_4)-(PO)(OH).[33] To our knowledge, this is the first time that they act as nonmagnetic spacers between magnetic units. It is such that the two types of Co---Co distances in adjacent chains are both sufficiently long (6.71 and 7.23 Å) to expect a magnetic disconnection through very weak *J* exchanges. Finally, in between the chains are large cages occupied by Ba^{II} and half of the water molecules which form H-bonds with O3 (d_{H2-O3} = 2.001 Å) (Figure 1a). The other half of the water molecules separate the layers along the a-axis, leading to Co−Co distances of 9.05 Å, which is sufficiently large to expect negligible magnetic interactions, especially in absence of any Co−$(O)_n$−Co orbital overlapping and available exchange path.

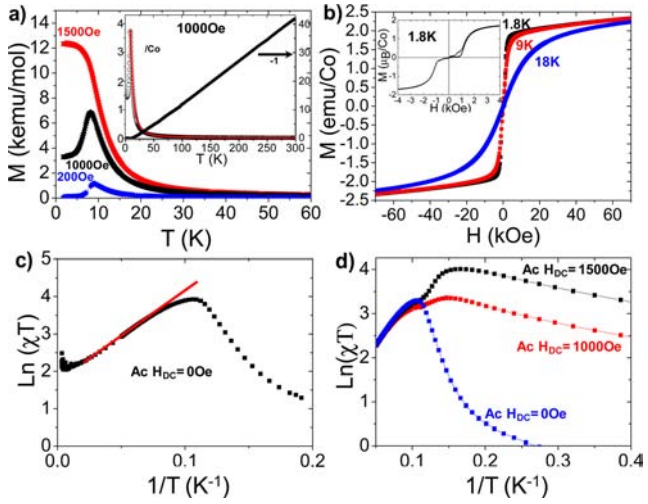

Figure 2. $BaCo_2(As_3O_6)_2 \cdot 2(H_2O)$ magnetic measurements. (Top) Direct current measurements with (a) temperature dependence of the dc magnetic susceptibility measured at 200, 1000, and 1500 Oe and corresponding inverse susceptibility and molar susceptibility fit in the inset, and (b) magnetization as a function of applied field at 2, 9, and 18 K and zoom-in on the low-field region at 1.8 K in the inset. (Bottom) Alternating current measurements with (c) $\ln(\chi T)$ vs $1/T$ plots with H_{dc} = 0 Oe, the solid line representing the linear fit, and (d) dependence of $\ln(\chi T)$ vs $1/T$ with H_{dc}.

Magnetic Properties. Figure 2a presents plots of χ and χ^{-1} (ZFC/FC curves) against temperature for $BaCo_2(As_3O_6)_2 \cdot 2(H_2O)_2$. There was no difference between the ZFC and FC curves. Between 50 and 300 K the linear $\chi^{-1}(T)$ plot was fitted by a Curie−Weiss equation,

$$\chi(T) = \frac{C}{T - \theta_{CW}}$$

where *C* is the Curie constant and θ_{CW} is the Weiss constant. For *H* = 1 kOe, it leads to μ_{eff} = 7.295 μ_B/f.u. (5.158 μ_B/Co^{II} and θ_{CW} = 21.4 K). One should note that, considering the predominant 1D magnetic character proved by upcoming

dx.doi.org/10.1021/ic402336n | *Inorg. Chem.* 2013, 52, 13742−13750

results, the Curie−Weiss law that is valid in the mean-field theory is not strictly appropriate but gives approximately quantitative results. In addition, due to our field-aligned sample, these values reflect parameters along the easy magnetic axis. Compared to the expected moment in a spin-only approximation (μ_{eff} = 3.87 μ_B/Co^{II}, S = 3/2, g = 2), the experimental μ_{eff} indicates an important orbital moment contribution, as expected for highly anisotropic magnetic Co^{II} ions. The positive Weiss constant indicates predominant positive exchanges between Co^{II} ions, most probably along the chain axis. Indeed, with respect to Kanamori−Goodenough rules, considering the superexchange path with Co−Co ≈ 3.02 Å and Co−O−Co ≈ 93°, the in-chain coupling is expected to be strong and ferromagnetic (FM). This was also experimentally evidenced by neutron diffraction in $BaCoAs_2O_7$[16] and $BiCoPO_5$,[34] which present similar edge-sharing connections between $Co^{II}O_6$ octahedra. In contrast, we have already suggested from structural features probable weak magnetic couplings. The $\chi(T)$ at 1 kOe above T = 10 K can be fitted using the Fisher 1D chain model (S = 3/2, $H = -JS_i \cdot S_j$) detailed in ref 35, giving $J_{Fischer}$ = 15.8(8) K and g = 2.32(6) (residual factor R = 3.2%), well-adapted to similar cases.[36] The result of the fit is shown in the inset of the Figure 2a. Similar values were fitted at 200 Oe. Once more, the handling of aligned susceptibility allows us to minimize perpendicular anisotropic contributions. Using the mean-field (MF) expression for the Curie−Weiss temperature, $\theta_{CW} = zJS(S+1)/3k_B$, where z is the number of Co neighbors along the chains (z = 2), leads to J_{MF} ≈ 8.6 K for S = 3/2. These results are in reasonable agreement if one considers the nonfrozen orbital contribution.

On further cooling, a broad but sharp peak occurs at ∼9 K (9.19 K measured ac susceptibility, dc-offset field = 0), after which $\chi(T)$ strongly depends on the applied field, as shown in Figure 2a. Below 0.1 T, it could be associated to a Néel-like 3D anti-ferromagnetic (AFM) ordering, even if the broad maximum suggests the progressive setting of short-range correlations. At higher field, the behavior changes into a FM-like aligned system which signs a metamagnetic transition occurring around 0.1 T, as expected in presence of disconnected magnetic chains likely for spin-flip transition. It is confirmed by the $M(H)$ curves at 1.8 K that show an abrupt magnetization step at 0.11 T, while the maximal moment value M_{max} = 4.65 μ_B/f.u. (at 5 T) is rapidly reached on increasing field. Note in the inset on Figure 2b the irreversibility of the first magnetization branch associated to minor grain reorientation and/or domain walls motion. Taking into account the particular $M(H)$ in the context of Co^{II} chains, the hypothesis for Ising chains is most probable, and the full chain-moment reversal at 0.1 and −0.1 T could be evoked. A similar but less abrupt $M(H)$ evolution is also observed at temperatures above the transition at T = 9 K, which suggest more dilute AFM interchain blocking effects. Figure 2b shows $M(H)$ at 1.8, 9, and 18 K. This phenomenon is nearly similar to what was observed in metamagnetic compounds with 1D nitronyl nitroxide-Tb^{III} chains[37] and mixed azide−carboxylate bridged Co^{II} chains[38] which combine AFM zero-field ordering and slow spin dynamics. To fully highlight this field-induced phenomenom, $M(H)$ and $\chi(T)$ plots have been combined to follow the characteristic field H_c in the (T,H) phase diagram. As shown in Figure 3, this characteristic field H_c is about 1100 Oe at 1.8 K and decreases continuously to vanish at 10 K. The shape by $H_c(T)$ is typical of paramagnetic (PM)−AFM transition line in metamagnetic materials.[39]

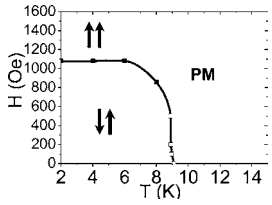

Figure 3. Phase diagram for $BaCo_2(As_3O_6)_2 \cdot 2(H_2O)$. Location of the maximum of susceptibility from (■) dM/dH vs H data and (□) χ vs T data. The solid line is a guide.

Estimation of *J*-Exchanges. To quantify the interactions in competition, we performed DFT calculations for various ordered magnetic states. Considering the spatially disconnected $(BaCo_2(As_3O_6)_2) \cdot H_2O$ units along the a-axis (Co−Co = 8.93 Å) the strongest hypothetical exchange path would correspond to Co-O-O_{As}-OH_2-O_{As}-O-Co, with $d(O_{As}-OH_2)$ = 3.3 Å, much greater than the sum of the van der Waals radii. So J_a can reasonably assumed as null and dominated by magnetic dipole−dipole interactions, as discussed below. In the layered units, on the basis of the shortest Co−Co interactions, we have considered two spin exchange parameters J_1 (nearest-neighbor in-chains along c) and J_2 (interchain interaction between two adjacent Co^{II} along b). The J_1 exchange path corresponds to a combination between Co−Co direct exchange and Co−O−Co superexchange (SE) as described in Table 2, while the next-nearest-neighbors (NNN) interaction along the chain has been neglected, generally weak in edge-sharing configuration (see the recent $BaFe_2(PO_4)_2$ case.[14] For J_2, the situation is more complicated since two distinct Co−Co distances coexist (J_{2a}, J_{2b}), but both involve the overlapping between three mediating oxygen atoms (Co−O−O−O−Co). J_{2a} and J_{2b} can then be approximated as equal and expected to be very weak compared to J_1 (see Table 2). Three magnetic configurations were defined in the original cell (see Figure S1), and the magnetic exchange parameters J_{1-2}, are then extracted by equating the relative energies of the three ordered magnetic states to the corresponding energies determined from the GGA+U calculation. Using U = 3 eV values, typically used for Co^{II} cations.[40,41] As expected, the interactions are found to be FM inside the chain (J_1 = 7.6 K) and weakly AFM between the chains (J_2 = −0.2 K), lower than our experimental estimations $J_{Fischer}$ = 15.8(8) K and J_{MF} ≈ 8.6 K. The lower value calculated by DFT includes the contribution of AFM and FM in-chain J_x, J_y, J_z accordingly to local magnetic anisotropy, while, once more, only the FM easy-axis is judged by magnetic measurement using an aligned sample, such that both $J_{Fischer}$ = 15.8(8) K and J_{MF} ≈ 8.6 K are overestimated because they are assigned to the FM-only component. In the presence of robust FM

Table 2. Description of Exchange Paths in $BaCo_2(As_3O_6)_2 \cdot 2(H_2O)_2$

	dCo−O (Å)	dO−O (Å)	dO−Co (Å)	J value at U = 3 eV (K)
J_1	2.079(9)		2.060(9)	**7.6**
	2.053(9)		2.060(9)	
J_{NNN}	2.079(9)	3.039(9)	2.053(9)	
J_{2a}	2.079(9)	2 × 2.614(9)	2.079(9)	**-0.2**
	2.073(9)	2 × 2.654(9)	2.073(9)	
J_{2b}	2.060(9)	2 × 2.614(9)	2.060(9)	
	2.375(9)	2 × 2.605(9)	2.375(9)	

dx.doi.org/10.1021/ic402336n | Inorg. Chem. 2013, 52, 13742−13750

chains, it is probable that the AFM couplings between them along *b* and *a* should be assisted by magnetic dipole−dipole interactions, as shown in Figure 4a. The subsequent possible ordering could respect the crystallographic unit-cell, taking into account that the next two chains along *a* and *b* form the lattice periodicity, but it is unstable under an external magnetic field.

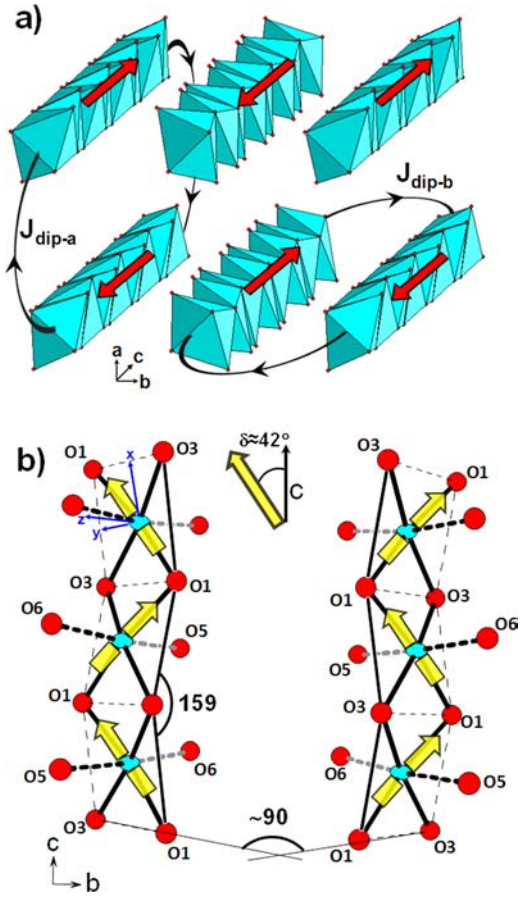

Figure 4. (a) Potential dipolar interactions in $BaCo_2(As_3O_6)_2{\cdot}2(H_2O)$. (b) Orientation of magnetic moments in $BaCo_2(As_3O_6)_2{\cdot}(H_2O)$ sheets.

Plausible Metamagnetic Scenario. In a uniaxial magnetic context favored by the Ising nature of the chains (as further demonstrated), the metamagnetic transition could reasonably be associated to a transition from AFM- to FM-aligned configuration between individual chains in the 2D units as shown on Figure 5. It is supported by energetic considerations since the critical field amplitude for the metamagnetic transition of $0.11T \approx 0.22$ K (at 1 T: 3 μ_BH # 0.174 meV # 2.01 K) is similar to the J_2 value (−0.2 K). Concerning the configuration between the 2D units, in the AFM state (H = 0), it is most probably driven by weak dipolar interactions (Co−Co = 8.93 Å), which favor a zero-field AFM arrangement between two stacked chains, see Figure 4a. At 14T, the magnetization reaches the value M_{max} = 2.33 μ_B/Co^{II}, which is less than expected for S = 3/2 ions with a large orbital contribution in case of parallel FM spin alignment. For instance, we have recently found for $BaCoP_2O_7$[16] (with a nearly equal effective moment in the PM regime, μ_{eff} = 5.1 μ_B/Co) a maximal magnetization of 3.35 μ_B/Co at 2 K and 14 T, consistent with the 3.7 μ_B/Co moment refined from neutron diffraction data. Quantitatively, in the title compound M_{max} would represent ~70% (= 2.33/3.35) of the expected saturated M_s value. The reason for this nonsaturated moment most probably stems from the unquenched Co^{II} orbital moment. Indeed, It is known that for isotropic magnetic cations, the spins are not influenced by the local orbital overlap, e.g., Fe^{III} (L = 0) magnetic moments are aligned along the *b*-axis of the triclinic unit-cell in $FeSO_4F$.[42] In contrast, for anisotropic ions the magnetic moments are influenced by the local crystal field as evidenced by the magnetic structure of the three following examples: (i) Spins of Fe^{II} (L = 2) ions in $LiFeSO_4F$ are aligned along the two and four local fold-axes of the FeO_6 octahedra.[42] (ii) Co^{II} (L = 3) spins in α-CoV_2O_6 are aligned along an octahedral O−Co−O diagonal perpendicular to the magnetic chains, while this orientation subsist to the field-induced ferrimagnetic and ferromagnetic transitions.[1,2] (iii) In $BaCoP_2O_7$, the Co^{II} (L = 3) spins are parallel to a Co−O bond of the basal O_4 plane, this orientation most probably being also conserved upon the field-induced magnetization steps.[16]

This orientation of moments driven by the local geometry for anisotropic ions was recently demonstrated using a quantum-mechanical approach for $_\infty[Co(H_2Z)(H_2O)]$ [Z = 4-Me-C_6H_4-

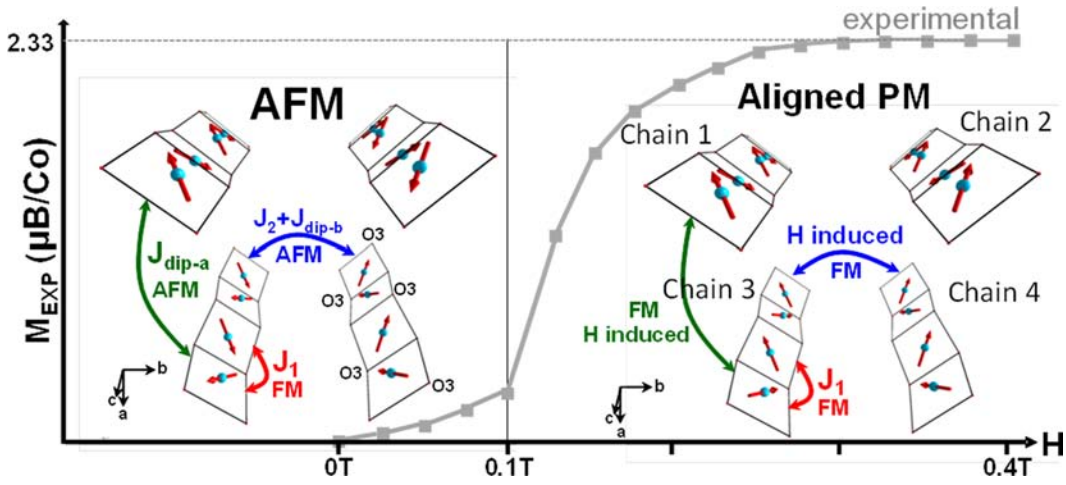

Figure 5. Model of metamagnetic transition with description of antiferromagnetic (AFM) and the canted FM-aligned configuration according to the magnetization shape. Only octahedral plane squares are represented to facilitate the comprehension.

dx.doi.org/10.1021/ic402336n | *Inorg. Chem.* 2013, 52, 13742−13750

Table 3. Description of the Irreducible Magnetic Representation Γ_3 (Space Group *Pnma*), k = (0,0,0), Which Corresponds to the Shubnikov Group *Pn′m′a*[a]

	Co1 x, y, z	Co2 $1/2 - x, -y, z + 1/2$	Co3 $x, 1/2 - y, z$	Co4 $1/2 - x, y + 1/2, z + 1/2$	Co5 $x + 1/2, y, 1/2 - z$	Co6 $-x, -y, -z$	Co7 $x + 1/2, 1/2 - y, 1/2 - z$	Co8 $-x, y + 1/2, -z$
M*x*	+	−	−	+	+	−	−	+
M*y*	+	−	+	−	+	−	+	−
M*z*	+	+	−	−	−	−	+	+
	Chain 1		Chain 2		Chain 3		Chain 4	
	Layer 1				Layer 2			

[a]This representation is compatible with the suggested AFM configuration at zero field. Labels Chain 1-4 refer to Figure 4.

$CH_2N(CPO_3H_2)_2]$.[43] In essence, it was shown in the concerned zigzag Co^{II} chains that the unquenched orbital moment and the strong axial crystal field are responsible for the spin orientation with respect to the local anisotropy axes. In the particular topology of these chains, it follows that the spins are tilted from one Co^{II} to the next one giving rise to an AFM canted structure with a nonvanishing magnetization. The corresponding deconvolution of the effective exchange, J_{eff}, into individual FM and AFM components along local axes (responsible for the canting) was analytically expressed and the authors validate their model in both AFM and FM J_{eff} cases.

Taking into account the octahedral geometry in the title compound, a similar tetragonal distortion than in $_\infty[Co(H_2Z)(H_2O)]$[43] is expected, with the O5−Co−O6 direction as the tetragonal axis. It follows that magnetic moments mediated by local crystal field is also expected. Indeed, as shown in Figure 4a, the hypothesis of spins mainly lying along either Co−O5 or Co−O6 directions is refuted since it would cancel the magnetization inside the chains. The most plausible scenario involves magnetic moments lying in the basal planes following either the O1−Co−O1 or O3−Co−O3 axis or any basal direction. As shown on the Figure 4b for the O1 choice, the tilting of spins along the chains implies two distinct components (FM along the local *x*-axis and AFM along the local *y*-axis) mediating the FM effective exchange J_1 (= J_{eff}) as predicted.[43]

If one assumes that the spins are lying along the O1−O1 diagonal of individual octahedra, one can estimate the resulting magnetization in both the AFM state (FM intrachains, AFM interchain along *b* and along *a*) and the FM-excited state (FM intrachain, FM interchains) with respect to symmetry, as follows: O1−O1 is taken as the magnetic spin unit using atomic coordinates, $\vec{S}_i = \overrightarrow{O1{-}O1} = 0.083\vec{a} + 0.1734\vec{b} + 0.5\vec{c}$, $|\vec{S}_i| = [(0.083a)^2 + (0.1734b)^2 + (0.5c)^2]^{1/2}$. Summing the magnetic components (average on eight individual tilted O1−O1 vectors in the unit cell) then leads to $\sum\vec{S}_l = 0\vec{a} + 0\vec{b} + 0\vec{c}$ for the AFM case, and $\sum\vec{S}_l = 0\vec{a} + 0\vec{b} + 0.5\vec{c}$ for FM case. In the latter model, an average vector $|\overrightarrow{S_{FM}}| = 0.734\ |\vec{S}_l|$ is found, very close to the 70% M_{max} announced above. In the $\vec{S}_l = \overrightarrow{O3{-}O3}$ hypothesis, one finds $|\overrightarrow{S_{FM}}| = 0.726\ |\vec{S}_l|$ also plausible. This scenario was validated by the calculations of magnetic dipole−dipole (MDD) interaction energies for three similar topologies (FM chains, AFM between next chains along the *a* and *b* axes, see Figure 4a) with moments parallel to *a*, *b*, and *c*. For this calculation, we sum all MDD interactions between spins S_i and S_j whose distances r_{ij} are shorter than 400 Å. The MDD interaction is given by[14]

$$\left(\frac{g^2\mu_B^2}{a_0^3}\right)\left(\frac{a_0}{r_{ij}}\right)^3[-3(\vec{S}_i\cdot\vec{e}_{ij})(\vec{S}_j\cdot\vec{e}_{ij}) + (\vec{S}_i\cdot\vec{S}_j)]$$

using $g = 2$, $S = 3/2$, $(g\mu_B)^2/a_0^3 = 0.725$ meV, $a_0 = 0.529177$ Å (Bohr radius), and $\mathbf{e}_{ij}$ the unit vector along r_{ij}. We find a stabilizing negative energy $E_{\|c} = -0.16$ meV/f.u., while it is destabilizing for perpendicular moments, e.g., $E_{\|a} = 0.07$ and $E_{\|b} = 0.09$ meV/f.u.

Finally about this point, assuming that the zero-field AFM state corresponds to magnetic ordering depicted above, and shown on the Figure 4, it is worth checking that the corresponding magnetic structure is allowed by group theory. Taking into account the eight individual Co^{II} atoms (8d site) in the unit cell disposed into four individual chains (two Co^{II} per chain), such an AFM alignment along *a* and *b* between canted FM chains corresponds to a propagation vector **k** = (0,0,0) with respect to the crystallographic unit cell. In other words, the AFM ordering periodicity conserves the crystallographic periodicity. Using BasIrep,[44] the global magnetic representation has been reduced upon eight irreducible representations each of them being one-dimensional:

$$\Gamma = 3\Gamma_1^{(1)} + 3\Gamma_2^{(1)} + 3\Gamma_3^{(1)} + 3\Gamma_4^{(1)} + 3\Gamma_5^{(1)} + 3\Gamma_6^{(1)} + 3\Gamma_7^{(1)} + 3\Gamma_8^{(1)}$$

The magnetic model corresponding to the AFM configuration (see Figure 4) is compatible with the irreducible representation Γ_3 described in Table 3 and Figure 4. This magnetic symmetry corresponds to the Shubnikov group *Pn′m′a*, as deduced from the characters of Γ_3.

Ising Chains. The one-dimensional behavior of $Ba-Co_2(As_3O_6)_2\cdot 2H_2O$ was checked following the correlation length, ξ, which is proportional to the χT product at zero dc field in any 1D classical system. The susceptibility of FM Ising chains (as well as anisotropic Heisenberg chains) shows an exponential divergence of the correlation length $\xi \propto \chi T = C\exp(\Delta_\xi/T)$, where Δ_ξ is the exchange energy cost to create domain walls along the chains.[45,46] It is worth noting that, in the case of noncolinear spins, the only accessible correlation is that of the noncompensated component of the magnetization (projected moment on the *c*-axis) as detailed in ref 47. However, in our case, both the noncompensated and chain axis coincide to the *c*-crystallographic axis. We plotted the $\ln(\chi' T)$ versus $1/T$, χ' being the magnetic susceptibility at 2.5 Oe (ac field) with an ac frequency of 1 Hz and zero dc field (see Figure 2c). It shows a linear region between 10 and 48 K, leading to $C = 3.3$ emu·K·mol^{-1} and $\Delta_\xi/k_b = 23.4$ K. In the Ising limit expected from the structural features and the strong spin−orbit coupling of Co^{II} ($\hat{H} = -\sum_{i<j}J_{ij}\hat{S}_i\cdot\hat{S}_j$), the gap Δ_ξ corresponds to $\Delta_\xi = 2J\cdot S^2\cos\delta$, where δ represents the canting angle between spins and the *c*-easy-axis, $\delta \approx 42°$ (see Figure 4a).[47] For

dx.doi.org/10.1021/ic402336n | Inorg. Chem. 2013, 52, 13742−13750

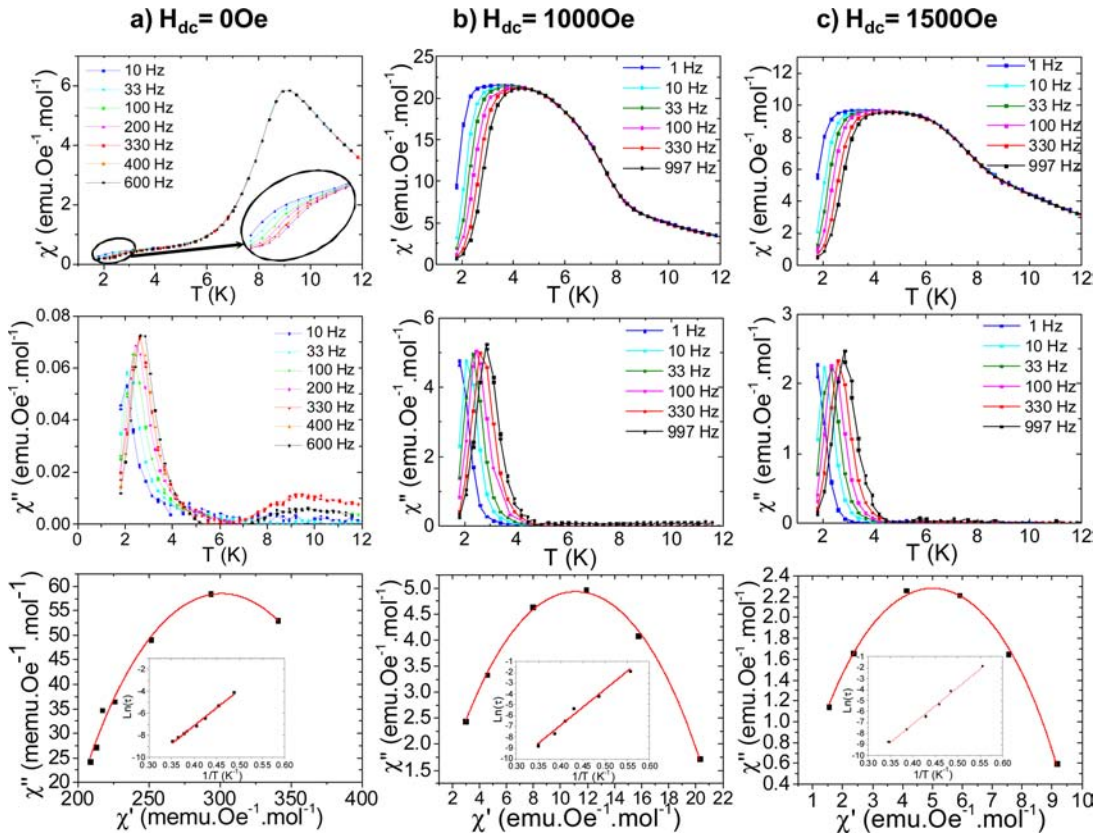

Figure 6. Ac susceptibilities of $BaCo_2(As_3O_6)_2{\cdot}2(H_2O)$ measured at different frequencies under different dc fields with a driving ac field of 2.5 Oe. For each dc field, the bottom figure corresponds to the Cole−Cole plot at 2.06 K for 0 Oe and at 2.35 K for 1000 and 1500 Oe, and the solid line is a least-squares fitting. The inset corresponds to the Arrhenius plot.

$BaCo_2(As_3O_6)_2{\cdot}2(H_2O)_2$, considering $S = 3/2$ ($Co^{II}(HS)$) and $J_1 = 7.6$ K from DFT calculation, Δ_ξ is calculated to be 25.3 K, in good agreement with experimental value, confirming the 1D Ising-like character. This value is comparable to results found for metamagnetic Ising Co^{II} chains with mixed azide−carboxylate bridges ($\Delta_\xi/k_b = 38.9$ K) in a noncanting system.[38] The Arrhenius plot at lower temperature also gives important insights about the real magnetic nature of the system in terms of interchain exchanges. For instance, comparison of $\ln(\chi T)$ vs $1/T$ plots of two distinct compounds with alternating chain repeating the [-Mn^{III}-ON-Ni^{II}-NO-] motif, has made it possible to distinguish between the finite size regime of SCM and an AFM order between SCM.[39] One behaves mainly as a paramagnet according to the saturated curve, whereas the other one exhibits an ordered AFM ground state between FM chains, giving rise to a drop of the $\ln(\chi T)$ vs $1/T$. A similar decrease was observed for the metamagnetic compound already mentioned above[38] between Ising Co^{II} chains with mixed azide−carboxylate bridges. As shown on the Figure 2d, in the title compound, the low-temperature domain is field-dependent. Below T_N, it reflects the phase diagram established before, since the applied dc field induces a change from pronounced χT decrease in zero-field (AFM ordering) toward an increase (spin alignment) below T_N.

Slow Spin Dynamics. To gain more insight into the magnetic characterization of the titled compound and validate the *H*-induced SCM behavior, thermal ac susceptibility measurements (Figure 6) were performed on aligned powder samples at zero field (AFM state), 1000 Oe (metamagnetic transition), and 1500 Oe dc field at various frequencies. Under zero field, the in-phase component, χ', exhibits a frequency-independent maximum at 9.2 K, with χ'' remaining null or very weak around this temperature, as expected for typical antiferromagnets. The weak χ'' peak shows an erratic evolution with frequency and should be ignored. Around 2−3 K, χ' shows a slight frequency dependence, while $\chi''T$ displays a frequency-dependent sharp peak. This behavior is indicative of slow relaxation effects, as for instance found in SCMs.[48−50] Under an applied dc field (Figure 6b,d), the *in-phase* susceptibility peak is broadened and displaced toward low temperatures, while the *out-of-phase* susceptibility remains nearly unchanged because the intrinsic chain dynamic is retained in the field-aligned PM state. The ϕ parameter, defined by $\phi = (\Delta T_p/T_p)/\Delta(\log f)$, where T_p is the peak temperature of the $\chi''T$ plot for each frequency,[51,52] has been used to estimate the frequency dependence found to be 0.13. This value is out of the range for spin glass but consistent with superparamagnets, including SCMs ($0.1 \leq \phi \leq 0.3$).[9,50] In other words, the slow spin dynamics is not suppressed in the AF state. Figure 6 shows the Cole−Cole plot of χ'' vs χ' at T= 2.05 K, which informs about the relaxation process. The semicircle shape indicates a single relaxation mode. It was fitted by a generalized Debye model using the equation from ref 52, considering a distribution of this single relaxation process. The pertinent α parameter can take values between 0 and 1 and gauges the width of the distribution ($\alpha = 1$ for a distribution of infinite width, while $\alpha = 0$ for the Debye form of single relaxation time). The fit leads to $\alpha = 0.6(1)$ at zero dc field, suggesting a large distribution of relaxation times compared to $\alpha \approx 0.1$ generally observed for real SCMs.[53,54] The broad distribution of relaxation times is

dx.doi.org/10.1021/ic402336n | Inorg. Chem. 2013, 52, 13742−13750

consistent with the wide shape of the ac susceptibility as a function of the temperature. Similar values have been found for $[Co(2,2'\text{-bithiazoline})(N_3)_2]_n$ SCM.[36] In our compound, even if the weak AFM ordering does not suppress the slow dynamics, it strongly disturbs it. To study the impact of the field on the relaxation process around the critical field, we have performed the same fit for dc field offsets of 1000 Oe (near to the transition) and 1500 Oe. Here also the semicircle (Figure 6) validates single mode. The fits yield $\alpha = 0.88(7)$ and 0.66(5) at 1000 and 1500 Oe, respectively. Near the critical field (1100 Oe), the increase of the distribution of relaxation times is consistent with a metamagnetic scenario breaking interchain AFM ordering, and impacting the relaxation process between them. So this broader distribution includes individual chain relaxations and perturbated ones due to the ongoing spin reversal. The energy barrier (Δ_τ) and the characteristic relaxation time (τ_o) for this system have been obtained by fitting (see insets of Cole−Cole plots, Figure 6) the temperature of the $\chi''T$ peak using an Arrhenius law, $\tau = \tau_o \exp(\Delta_\tau/T)$. Experimentally, τ could be deduced from the maximum of χ'', leading to $\tau_o = 1.83 \times 10^{-9}$ s and $\Delta_\tau = 32.5$ K at $H_{dc} = 0$, which validates the thermally activated relaxation and slow spin dynamics. Under dc field offsets, comparable values for the activation energy Δ_τ are obtained, while τ_o decreases slightly with the applied field [$\tau_o = 1.65 \times 10^{-9}$ s and $\Delta_\tau = 33.7$ K at $H_{dc} = 1000$ Oe; $\tau_o = 1.15 \times 10^{-9}$ s and $\Delta_\tau = 33.5$ K at $H_{dc} = 1500$ Oe] and falls close to values found for other magnetic Co^{II} chain compounds (i.e., $\tau_o = 2.5 \times 10^{-10}$ s and $\Delta_\tau = 49.2$ K in $[Co(N_3)(COO)_2]_n$ chains[38]). This is at variance with the results reported for other SCM compounds with non-null magnetization.[55] In our case, it looks like the metamagnetic transition induces a broadening of the relaxation time distribution (α effect), while the applied field shifts the characteristic time to lower values. Similar observations in AFM chain systems led other authors to conclude that the AFM ordering imposes an internal field and modifies the SCM component.[38] Finally in the "finite-size-chain" regime, the Glauber dynamics for FM Ising chains predicts that the activation barrier $\Delta_\tau = \Delta_\xi$, where the increase of ξ is limited by defects.[38] In our case the difference between Δ_τ (32.5 K) and Δ_ξ (23.4 K) corresponds to the fact that the Ising model is an idealized limiting case, and in real systems, the spin flip in the absence of magnetic exchange is also thermally activated with an anisotropy gap, Δ_a, such that $\Delta_\tau = \Delta_\xi + \Delta_a$.[39] We find $\Delta_A = 9.1$ K, very similar to the 10 K values found for other Co^{II} chain-like compounds, which also have an AFM ground state.[38]

CONCLUSION

Using hydrazine as reducing agent in hydrothermal conditions, we stabilized the second example of Co^{II}/As^{III} oxide: $BaCo_2(As_3O_6)_2{\cdot}2(H_2O)_2$. It consists of highly disconnected $BaCo_2(As_3O_6)_2{\cdot}2(H_2O)$ units formed of infinite edge sharing CoO_6 chains linked by complex and rare chains of corner-sharing AsO_3 groups. Magnetic study has allowed us to highlight a metamagnetic transition around 0.1 T up to 70% of the expected saturation. To explain the later, we have proposed a model based on the results of DFT calculations and the decomposition of magnetic representations using group theory. We demonstrate that our compound fulfills most requirements as described in the literature[6] to be considered as a single-chain magnet (SCM). Indeed, it consists of ferromagnetic canted isolated chains. The interchain interactions are negligible in comparison with ferromagnetic intrachain interactions, while a pronounced uniaxial anisotropy in the octahedral crystal field is favored. However, although slow relaxation of the magnetization has a weak influence on the dc field, interchains AFM couplings avoid freezing a nonzero magnetization at zero field. Therefore, although the title compounds exhibits most characteristics of a SCM, it lacks a spontaneous magnetization to be properly called a magnet.[56] The originality of the title compound mainly stems from its "pure" inorganic nature, in contrast to most commonly found hybrid organic/inorganic SCMs. In that sense, similarities with $Ca_3Co_2O_6$ can be established. In this latter disconnected FM Co^{II}, chains are arranged into a frustrated triangular lattice, which also create slow spin dynamics.[57] The spin dynamics of $Ca_3Co_2O_6$ have been analyzed by ac magnetic susceptibility. In zero field, the temperature dependence of the spin-relaxation time shows a crossover between an activated (Arrhenius-like) regime above $T_{cross} = 8$ K and a quantum (T-independent) regime above T_{cross}, consistent with the quantum tunneling of the magnetization with regular magnetization steps. The difference in behavior between the title metamagnetic compound and $Ca_3Co_2O_6$ most probably arises from the larger disconnection between chains in the latter, in the absence of a frustrated topology.

ASSOCIATED CONTENT

Supporting Information

Single-crystal XRD data, refined positions, anharmonic displacement parameters, and description of magnetic configurations used for J calculation. This material is available free of charge via the Internet at http://pubs.acs.org.

AUTHOR INFORMATION

Corresponding Author

*E-mail: olivier.mentre@ensc-lille.fr.

Notes

The authors declare no competing financial interest.

ACKNOWLEDGMENTS

This work was carried out under the framework of the MADBLAST project supported by the ANR (Grant ANR-09-BLAN-0187-01). The Fonds Européen de Développement Régional (FEDER), CNRS, Région Nord Pas-de-Calais, and Ministère de l'Enseignement Supérieur et de la Recherche are acknowledged for funding of the X-ray diffractometers. R.D. thanks the ENS of Lyon for financial support.

REFERENCES

(1) Lenertz, M.; Alaria, J.; Stoeffler, D.; Colis, S.; Dinia, A.; Mentré, O.; André, G.; Porcher, F.; Suard, E. *Phys. Rev. B* **2012**, *86*, 214428.
(2) Markkula, M.; Arévalo-López, A. M.; Attfield, J. P. *Phys. Rev. B* **2012**, *86*, 134401.
(3) Zhao, Y.; Gong, S.-S.; Li, W.; Su, G. *Appl. Phys. Lett.* **2010**, *96*, 162503.
(4) Sessoli, R.; Gatteschi, D.; Caneschi, A.; Novak, M. A. *Nature* **1993**, *365*, 141−143.
(5) Sessoli, R.; Tsai, H. L.; Schake, A. R.; Wang, S.; Vincent, J. B.; Folting, K.; Gatteschi, D.; Christou, G.; Hendrickson, D. N. *J. Am. Chem. Soc.* **1993**, *115*, 1804−1816.
(6) Caneschi, A.; Gatteschi, D.; Lalioti, N.; Sangregorio, C.; Sessoli, R.; Venturi, G.; Vindigni, A.; Rettori, A.; Pini, M. G.; Novak, M. A. *Angew. Chem., Int. Ed.* **2001**, *40*, 1760−1763.
(7) Clérac, R.; Miyasaka, H.; Yamashita, M.; Coulon, C. *J. Am. Chem. Soc.* **2002**, *124*, 12837−12844.

(8) Lescouëzec, R.; Vaissermann, J.; Ruiz-Pérez, C.; Lloret, F.; Carrasco, R.; Julve, M.; Verdaguer, M.; Dromzee, Y.; Gatteschi, D.; Wernsdorfer, W. *Angew. Chem., Int. Ed.* **2003**, *42*, 1483−1486.
(9) Sun, H.-L.; Wang, Z.-M.; Gao, S. *Coord. Chem. Rev.* **2010**, *254*, 1081−1100.
(10) Eymond, S.; Martin, M. C.; Durif, A. *Mater. Res. Bull.* **1969**, *4*, 595−599.
(11) Heinrich, M.; Krug von Nidda, H.-A.; Loidl, A.; Rogado, N.; Cava, R. J. *Phys. Rev. Lett.* **2003**, *91*, 137601.
(12) Regnault, L. P.; Burlet, P.; Rossat-Mignod, J. *Phys. BC* **1977**, *86−88* (Part 2), 660−662.
(13) Regnault, L. P.; Rossat-Mignod, J. In *Magnetic Properties of Layered Transition Metal Compounds*; De Jongh, L. J., Ed.; Kluwer: Dordrecht, 1990.
(14) Kabbour, H.; David, R.; Pautrat, A.; Koo, H.-J.; Whangbo, M.-H.; André, G.; Mentré, O. *Angew. Chem., Int. Ed.* **2012**, *51*, 11745−11749.
(15) David, R.; Kabbour, H.; Pautrat, A.; Mentré, O. *Inorg. Chem.* **2013**, *52*, 8732−8737.
(16) David, R.; Kabbour, H.; Colis, S.; Pautrat, A.; Suard, E.; Mentré, O. *J. Phys. Chem. C* **2013**, *117*, 18190−18198.
(17) Yakubovich, O. V.; Karimova, O. V.; Dimitrova, O. V.; Massa, W. *Acta Crystallogr. C* **1999**, *55*, 151−153.
(18) Bu, X.; Feng, P.; Stucky, G. D. *J. Solid State Chem.* **1997**, *131*, 387−393.
(19) Le Meins, J.-M.; Grenèche, J.-M.; Courbion, G. *J. Solid State Chem.* **1999**, *148*, 286−294.
(20) Hamida, B. Oxo-Selenate(IV) und Oxo-Arsenate(III) der Selten-Erd-Metalle und ihre Derivate.Ph.D. thesis, Universität Oldenburg, 2007.
(21) Lösel, S.; Hillebrecht, H. *Z. Anorg. Allg. Chem.* **2008**, *634*, 2299−2302.
(22) Weast, R. C. *CRC Handbook of Chemistry & Physics*, 53rd ed.; Chemical Rubber Co.: Cleveland, OH, 1972.
(23) *SADABS*: Area-Detector Absorption Correction; Siemens Industrial Automation, Inc.: Madison, WI, 1996.
(24) Palatinus, L.; Chapuis, G. *J. Appl. Crystallogr.* **2007**, *40*, 786−790.
(25) Petricek, V.; Dusek, M.; Palatinus, L. *JANA2000*: The Crystallographic Computing System; Institute of Physics: Praha, Czech Republic, 2000.
(26) Kresse, G.; Furthmüller, J. *VASP*: Vienna Ab-initio Simulation Package; Institut für Materialphysik: Vienna, 2004; http://cms.mpi.univie.ac.at/vasp.
(27) Perdew, J. P.; Wang, Y. *Phys. Rev. B* **1992**, *45*, 13244−13249.
(28) Kresse, G.; Joubert, D. *Phys. Rev. B* **1999**, *59*, 1758−1775.
(29) Klaska, R.; Gebert, W. *Z. Krist. Krist. Krist. Krist.* **1982**, *159*, 75.
(30) Ben Harmida, M.; Warns, C.; Wickleder, M. S. *Z. Naturforsch.* **2005**, *60b*, 1219−1223.
(31) Lee, C.; Harrison, W. T. A. *Acta Crystallogr. C* **2004**, *60*, 215−218.
(32) Ghose, S.; Sen Gupta, P. K.; Schlemper, E. O. *Am. Mineral.* **1987**, *72*, 629−632.
(33) Bondenstein, D.; Brehm, A.; Jones, P. G.; Schwarzmann, E.; Sheldrick, G. M. *Z. Naturforsch. B: Anorg. Chem. Org. Chem.* **1982**, *37*, 531.
(34) Mentre, O.; Bouree, F.; Rodriguez-Carvajal, J.; Jazouli, A. E.; Khayati, N. E.; Ketatni, E. M. *J. Phys.: Condens. Matter* **2008**, *20*, 415211.
(35) Fisher, M. E. *Am. J. Phys.* **1964**, *32*, 343.
(36) Liu, T.-F.; Fu, D.; Gao, S.; Zhang, Y.-Z.; Sun, H.-L.; Su, G.; Liu, Y.-J. *J. Am. Chem. Soc.* **2003**, *125*, 13976−13977.
(37) Liu, R.; Zhang, C.; Mei, X.; Hu, P.; Tian, H.; Li, L.; Liao, D.; Sutter, J.-P. *New J. Chem.* **2012**, *36*, 2088−2093.
(38) Zhang, X.-M.; Wang, Y.-Q.; Wang, K.; Gao, E.-Q.; Liu, C.-M. *Chem. Commun.* **2011**, *47*, 1815−1817.
(39) Miyasaka, H.; Takayama, K.; Saitoh, A.; Furukawa, S.; Yamashita, M.; Clérac, R. *Chem.—Eur. J.* **2010**, *16*, 3656−3662.
(40) Walsh, A.; Wei, S.-H.; Yan, Y.; Al-Jassim, M.; Turner, J.; Woodhouse, M.; Parkinson, B. *Phys. Rev. B* **2007**, 76.
(41) Dalverny, A.-L.; Filhol, J.-S.; Lemoigno, F.; Doublet, M.-L. *J. Phys. Chem. C* **2010**, *114*, 21750−21756.
(42) Melot, B. C.; Rousse, G.; Chotard, J.-N.; Ati, M.; Rodríguez-Carvajal, J.; Kemei, M. C.; Tarascon, J.-M. *Chem. Mater.* **2011**, *23*, 2922−2930.
(43) Palii, V.; et al. *J. Am. Chem. Soc.* **2008**, *130*, 14729−14738.
(44) Rodriguez-Carvajal, J. *BasIrep*: a Program for Calculating Irreductible Representations of Little Groups and Basis Functions of Polar and Axial Vector Properties; ILL: Grenoble, 2004.
(45) Loveluck, J. M.; Lovesey, S. W.; Aubry, S. *J. Phys. C Solid State Phys.* **1975**, *8*, 3841.
(46) Nakamura, K.; Sasada, T. *J. Phys. C Solid State Phys.* **1978**, *11*, 331.
(47) Bernot, K.; Luzon, J.; Sessoli, R.; Vindigni, A.; Thion, J.; Richeter, S.; Leclercq, D.; Larionova, J.; van der Lee, A. *J. Am. Chem. Soc.* **2008**, *130*, 1619−1627.
(48) Bogani, L.; Sangregorio, C.; Sessoli, R.; Gatteschi, D. *Angew. Chem., Int. Ed.* **2005**, *44*, 5817−5821.
(49) Žumer, S. *Phys. Rev. B* **1980**, *21*, 1298−1303.
(50) Coulon, C.; Miyasaka, H.; Clérac, R. Single-Chain Magnets: Theoretical Approach and Experimental Systems. In *Single-Molecule Magnets and Related Phenomena*; Winpenny, R., Ed.; Structure and Bonding; Springer: Berlin/Heidelberg, 2006; pp 163−206.
(51) Pardo, E.; Train, C.; Lescouëzec, R.; Journaux, Y.; Pasán, J.; Ruiz-Pérez, C.; Delgado, F. S.; Ruiz-Garcia, R.; Lloret, F.; Paulsen, C. *Chem. Commun. (Cambridge)* **2010**, *46*, 2322−2324.
(52) Visinescu, D.; Madalan, A. M.; Andruh, M.; Duhayon, C.; Sutter, J.-P.; Ungur, L.; Van den Heuvel, W.; Chibotaru, L. F. *Chem.—Eur. J.* **2009**, *15*, 11808−11814.
(53) Ishikawa, R.; Katoh, K.; Breedlove, B. K.; Yamashita, M. *Inorg. Chem.* **2012**, *51*, 9123−9131.
(54) Kajiwara, T.; Tanaka, H.; Yamashita, M. *Pure Appl. Chem.* **2008**, *80*, 2297−2308.
(55) Coulon, C.; Clérac, R.; Wernsdorfer, W.; Colin, T.; Miyasaka, H. *Phys. Rev. Lett.* **2009**, *102*, 167204.
(56) Glauber, R. J. *J. Math. Phys.* **1963**, *4*, 294−307.
(57) Hardy, V.; Lees, M. R.; Petrenko, O. A.; Paul, D. M.; Flahaut, D.; Hebert, S.; Maignan, A. *Phys. Rev. B Condens. Matter Mater. Phys.* **2004**, *70*, 064424.1−064424.7.